Supplementary Information for "Decoupling of rates of protein synthesis from cell expansion leads to supergrowth"

Benjamin D. Knapp[1,2], Pascal Odermatt[1,3], Enrique R. Rojas[3,4], Wenpeng Cheng[5], Xiangwei He[5], Kerwyn Casey Huang[2,3,6,7,*], and Fred Chang[1,*]

[1]Department of Cell and Tissue Biology, University of California, San Francisco, San Francisco, CA 94143

[2]Biophysics Program, Stanford University, Stanford, CA 94305, USA

[3]Department of Bioengineering, Stanford University, Stanford, CA 94305, USA

[4]Department of Biochemistry, Stanford University School of Medicine, Stanford, CA 94305, USA

[5]Life Sciences Institute, Zhejiang University, Hangzhou, Zhejiang, China, 310027

[6]Department of Microbiology and Immunology, Stanford University School of Medicine, Stanford, CA 94305, USA

[7]Chan Zuckerberg Biohub, San Francisco, CA 941586

[*]To whom correspondence should be addressed:

Fred Chang

513 Parnassus Avenue

San Francisco, CA 94143 USA

Phone: +1 (415) 476-8922

E-mail: fred.chang@ucsf.edu

Kerwyn Casey Huang

Shriram Center, Room 007 MC: 4245

443 Via Ortega

Stanford, CA 94305-4125 USA

Phone: +1 (650) 721-2483

E-mail: kchuang@stanford.edu

Supplemental Figures

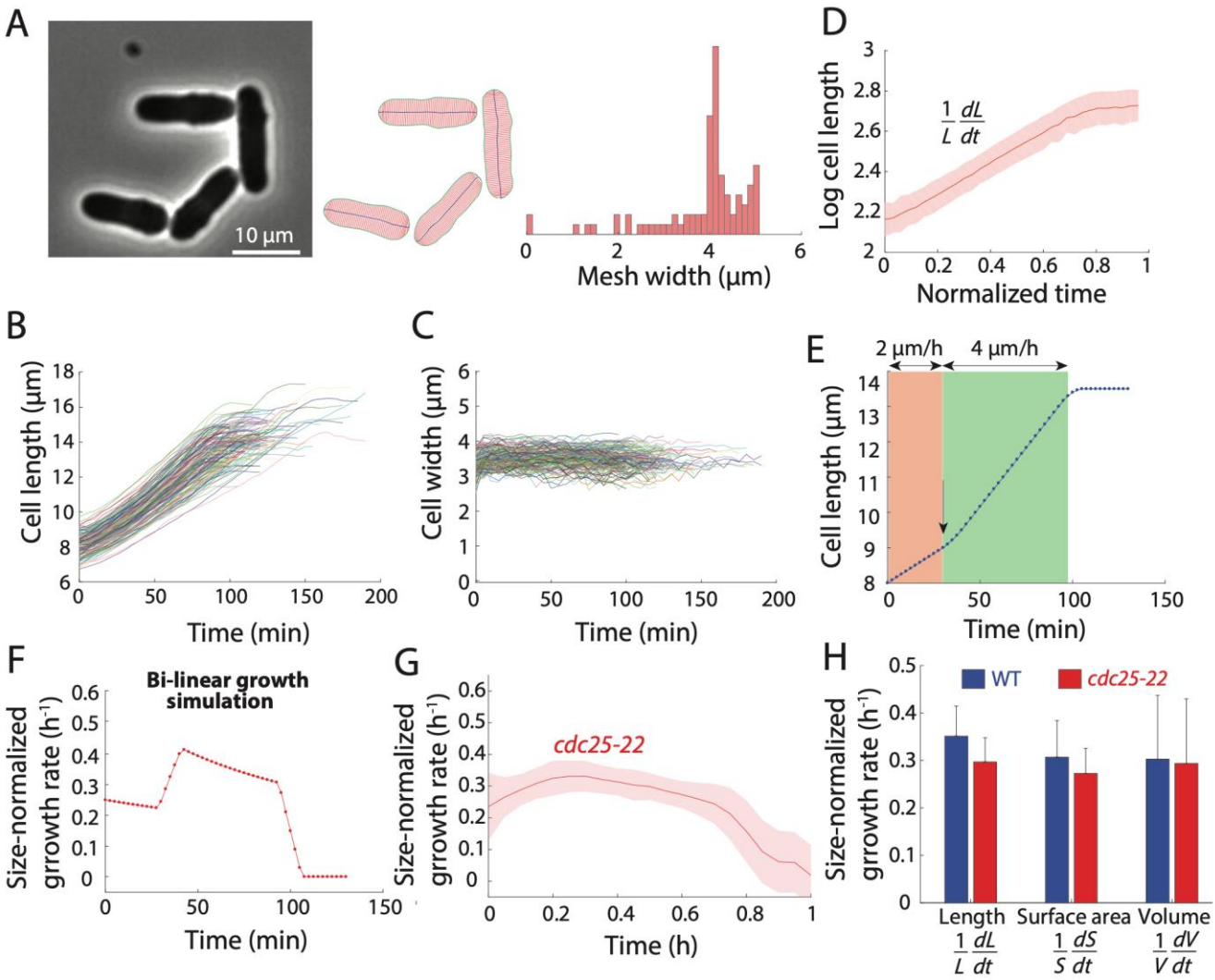

Figure S1: *S. pombe* cells exhibit exponential growth for a large fraction of the cell cycle. (Related to Figure 1)

A) Example of phase-contrast image of cells grown in microfluidic chambers (left) and skeleton (middle; red: width, green: outline, blue: centerline) calculated from automated segmentation analysis (Methods). Right: the distribution of mesh widths

of an example skeleton, with the overall cell width defined as the median of this distribution.

B) Cell length traces of a population of wild-type cells during steady-state growth in a microfluidic flow cell. Cell growth rate decreases in mitosis and cytokinesis (n = 147 cells).

C) Cell width traces of the population of wild-type cells shown in (B).

D) Logarithm of the length of wild-type cells during steady-state growth plotted against the normalized time between divisions. The linear portion corresponds to exponential growth (n = 1129 cells).

E) Simulation of bilinear growth according to growth rates and transition times proposed in the literature (Baumgartner and Tolic-Norrelykke, 2009; Cooper, 2006; Mitchison and Nurse, 1985; Sveiczer et al., 1996). Cells were assumed to elongate at 2 μm/h for the first third of G2 and then elongation rate doubled to 4 μm/h until starting mitosis at 14 μm.

F) The size-normalized growth rate of a cell undergoing bilinear growth as in (E) is clearly incongruent with our experimental measurements (compare with Figure 1C).

G) Size-normalized growth rate ($1/L\ dL/dt$) of *cdc25-22* cells during steady-state growth, excluding mitosis. Shading represents ± one standard deviation (S.D.) (n = 246 cells).

H) Size-normalized growth rates as measured from length (L), surface area (S), or volume (V). Error bars represent ±1 S.D.

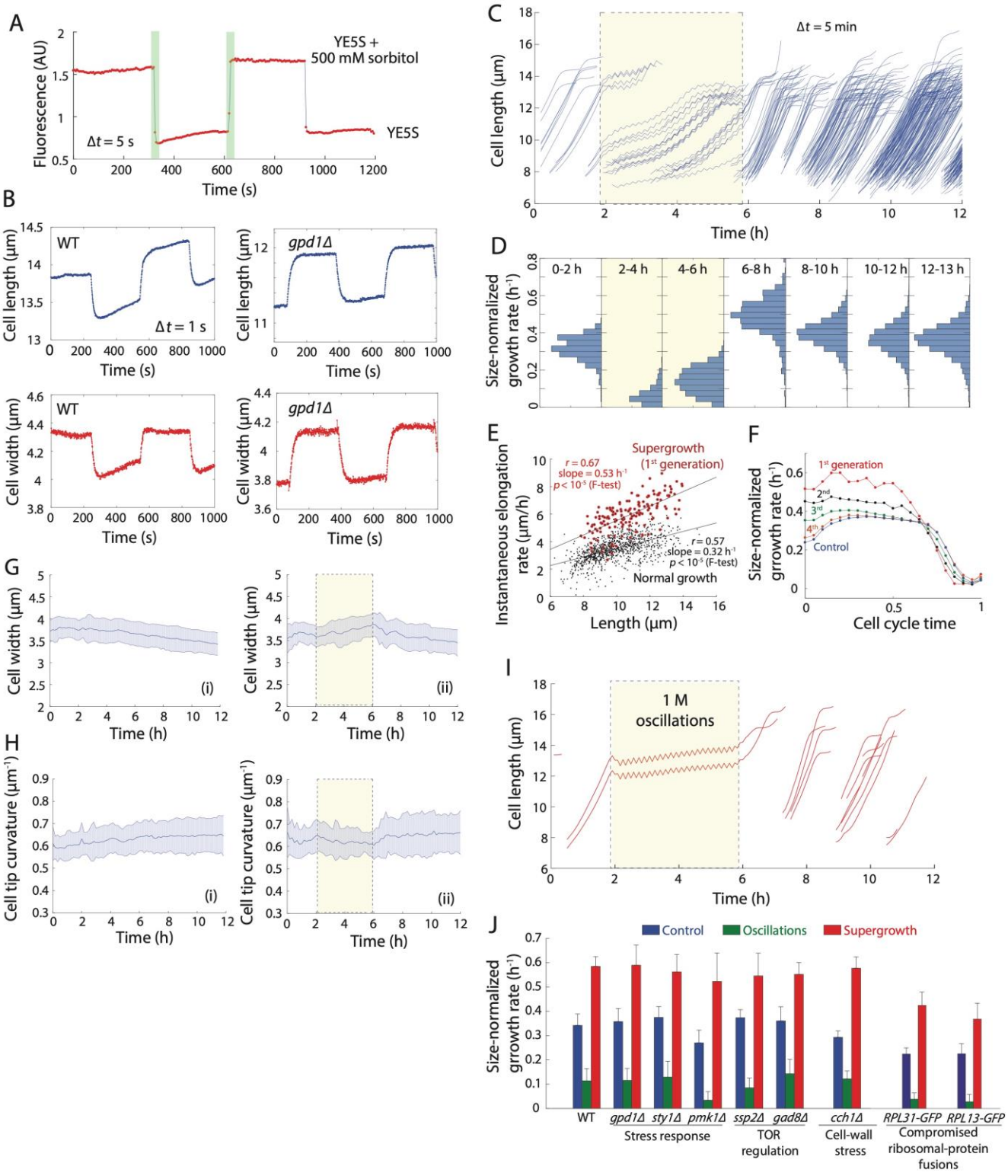

Figure S2: Supergrowth does not affect cell size and cell-cycle regulation, and is not dependent on stress response and TOR pathways. (Related to Figures 2-4)

A) Oscillatory media exchange is rapid in microfluidic device. CellAsic chip was loaded with YE5S and subjected to oscillations with YE5S plus tracer dye (0.5 μg/mL Alexa Fluor 647 carboxylic acid) and 0.5 M D-sorbitol (10-min period). Fluorescence images (YFP) acquired every 5 s demonstrated that the media were exchanged in less than 10 s.

B) Response of wild-type cells and a *gpd1Δ* mutant defective in osmotic adaptation. Cell length (blue) and width (red) of a representative wild-type (left) and *gpd1Δ* (right) cell during oscillatory 0.5 M sorbitol osmotic shocks with 10-min period. *gpd1Δ* lack the recovery in cell width that occurs in wildtype after hyperosmotic shocks. Images were acquired every 1 s.

C) Effect of oscillations on cell growth. Length trajectories of wild-type cells undergoing oscillatory osmotic shocks. Yellow outlined box represents the 4-h duration of 0.5 M D-sorbitol shocks with 10-min period. Images were acquired every 5 min (n = 302 cells).

D) Effect of oscillations on growth rate. Histograms of size-normalized growth rates during a typical oscillation experiment (500 mM sorbitol, 10-min period, 4 h; yellow background). Each time window corresponds to either 1 or 2 h durations, in which size-normalized growth rates were binned. The total number of cells n = 929; N = 399, 725, 1034, 233, 1028, 3594, 4394 data points in each time window.

E) Growth rate during the first cell cycle of supergrowth is higher than during steady-state growth. Instantaneous elongation rate increases with cell length during the first generation of supergrowth (red circles; n = 159). The slope of the best linear fit

is steeper than that of normal growth (black dots; *n* = 998), indicating a higher size-normalized growth rate.

F) Cells exhibit exponential growth during supergrowth. Size-normalized growth rates as a function of normalized cell-cycle time during each generation of supergrowth after 4-h of oscillatory 0.5 M D-sorbitol osmotic shocks with 10-min period. The first generation of supergrowth represents cells that divided within 15 min of exit from oscillations (*n* = 10 cells). Subsequent generations were classified based on manual inspection of trajectories. The second generation of supergrowing cells did not display the initial phase of super-exponential growth (Figure 1C). Number of cells *n* (generation): 146 (2^{nd}), 194 (3^{rd}), 298 (4^{th}), 929 (control).

G) Cell width remains approximately constant during oscillations. Cell width measurements during normal growth (left) and osmotic shock oscillations (right; yellow box represents 4 h of 0.5-M sorbitol oscillations with 10-min period). Apparent decreases in width during normal growth were due to cell crowding effects on automatic segmentation. Dark centerline is the population-averaged mean width and the shading represents ±1 S.D. (control, *n* = 1242 cells; oscillations, *n* = 973 cells).

H) Cell tip shape remains approximately constant during oscillations. Cell tip curvature measurements during normal growth (left) and osmotic shock oscillations (right; yellow box represents 4 h of 0.5-M sorbitol oscillations with 10-min period). Dark centerline is the population-averaged mean cell tip curvature and the shading represents ±1 S.D. (control, *n* = 1242 cells; oscillations, *n* = 973 cells).

I) Some cells transit 1 M oscilations without dividing and exhibit subsequent supergrowth. Cell length across the progeny of an inital cell during a large-amplitude oscillation experiment (1 M sorbitol, 10-min period, 4 h; yellow box). During oscillations, volume growth was reduced to approximately zero, allowing individual cells to traverse the entire duration of oscillations without division. These cells still underwent supergrowth. Incomplete trajectories during oscillations were due to errors in tracking (*n* = 17 cells).

J) Supergrowth is independent of stress response pathways and TOR pathways. Mutants in stress response pathways and growth regulation were tested for response to oscillations. The ribosomal protein GFP fusions were examined as examples of slow growth ribosomal mutants. Control and oscillatory elongation rates were computed as the mean size-normalized growth rates during steady-state growth prior to osmotic shocks and during the 4 h of oscillations, respectively; supergrowth rate was defined as the peak in the growth rate after exit from oscillations, smoothed over a 15-min time window. Error bars represent ±1 S.D. Number of cells: WT, *n* = 929; *gpd1Δ*, *n* = 641; *sty1Δ*, *n* = 395; *pmk1Δ*, *n* = 421; *ssp2Δ*, *n* = 443; *gad8Δ*, *n* = 634; *cch1Δ, n* = 197; *RPL31-GFP*, *n* = 99; *RPL13-GFP*, *n* = 62.

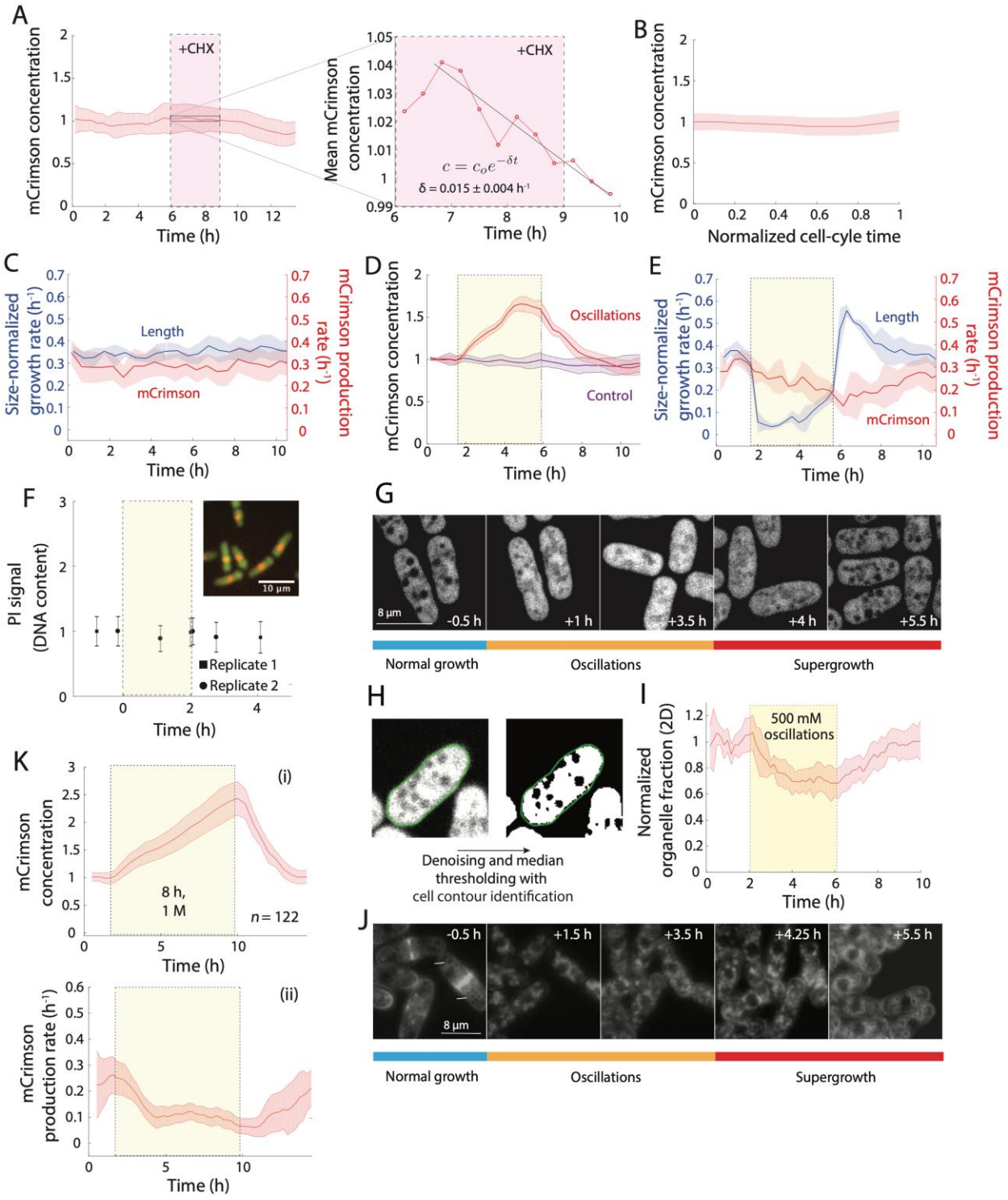

Figure S3: Decoupling of protein production from volume growth leads to an increase in global protein concentration. (Related to Figure 5)

A) mCrimson is stable. Left: Cells expressing mCrimson were grown in microfluidic chambers with YE5S and then exposed to a pulse of YE5S with 100 μg/mL cycloheximide (CHX) for 3 h. (Right) The mean mCrimson concentration decreased by <5% during the 3 h treatment with CHX, indicating a degradation rate of 0.015 h^{-1}, within experimental noise. Shaded error bars represent ±1 S.D. (n = 260 cells).

B) mCrimson is normally maintained at a constant concentration throughout the cell cycle during steady-state growth (n = 254 cells). t = 0 represents the birth time, and time is normalized to the time between birth and division (as defined by 'snapping'). Dark line is the population mean and shaded bars represent ±1 S.D.

C) Population-averaged mCrimson production rate and size-normalized growth rate were approximately constant during steady-state growth (excluding mitosis). Fluorescence production rate was defined as the instantaneous cellular change in the log of the integrated intracellular fluorescence. Shaded bars represent ±1 S.D. (n = 254 cells).

D) mCrimson concentration rises during oscillations. Population-averaged intracellular concentration of mCrimson during growth (excluding mitosis). Cells undergoing osmotic shock oscillations (red) increased their mCrimson concentrations by ~60% relative to control cells (purple) over the course of the oscillations. Yellow outlined box represents the 4-h duration of 0.5-M sorbitol osmotic shocks with 10-min period. Control cells were grown in a chamber of the same microfluidic flow cell adjacent to cells exposed to oscillations. Shaded bars represent ±1 S.D. (n = 842 cells).

E) Rate of mCrimson synthesis does not rise during oscillations. Population-averaged mCrimson production rate and elongation rate (excluding mitosis) during an oscillatory osmotic shock experiment. Yellow outlined box represents the 4-h duration of 0.5 M D-sorbitol shocks with 10-min period. Shaded bars represent ±1 S.D. (n = 842 cells).

F) DNA levels are stable during oscillations and supergrowth. Propidium iodide (PI) staining, which was used to estimate cellular DNA content (Methods), remained constant throughout both osmotic shock oscillations and supergrowth in non-mitotic cells. The yellow outlined box indicates 12 cycles of 500 mM sorbitol shocks with 10-min period (STAR Methods). Error bars are ±1 S.D. (n > 2000 cells).

G-I) Measuring changes in vacuolar volume from mCrimson fluorescence. (G) Images of cells expressing mCrimson before, during, and after 500 mM oscillations. Dark regions of excluded fluorescence are assumed to be non-nuclear organelles; the large majority of these organelles are vacuoles (Parkinson et al., 2008). Time is relative to when oscillations started. (H) Method for estimating vacuolar fraction. The extent to which vacuoles took up cytoplasmic volume was roughly estimated as the two-dimensional cross-sectional area of fluorescence exclusion (dark round structures in (G)). Fluorescence images were de-noised, and then a median threshold was applied to obtain mCrimson-excluded regions. These binary images were used to compute the organelle fraction as the ratio of dark to light pixels within the contour. Contours (green line) were extracted from the fluorescence images using *Morphometrics*. (I) Estimated vacuolar volume changes during oscillations. Using the method described in (G, H), time-lapse images were analyzed

before, during, and after exposure to osmotic oscillations (500 mM D-sorbitol, 10 min period, 4 h; light yellow box). The dark line corresponds to the population average and the shaded regions represent ±1 S.D. (n = 130 cells). These data show that the vacuolar fraction decreased ~30% during oscillations. Considering that vacuoles make up approximately 10% of the cytoplasmic volume of yeast cells (Parkinson et al., 2008), changes in vacuolar volume can represent only ~3% of total volume and thus cannot account for the cell density changes observed during oscillations.

J) Vacuolar staining using FM4-64. Cells were exposed to osmotic oscillations (500 mM D-sorbitol, 10 min period, 4 h) and stained with the membrane dye FM4-64. Arrows in the first image indicate vacuoles, which became fragmented and small during oscillations. Vacuole shape and size recovered approximately 90 min post-oscillations. Time is relative to when oscillations started.

K) A higher concentration (1 M) of sorbitol during oscillations leads to larger increases in mCrimson concentration. Top: Concentration of mCrimson during a long-duration (8 h) osmotic shock oscillation experiment with large-amplitude (1 M) shocks with 10-min period. Bottom: After an initial decrease over the first 2 h, mCrimson production stabilized at a rate ~0.1 h^{-1} and persisted throughout the rest of the oscillations. The centerline is the population average, and shaded error bars are ±1 S.D. (n = 122 cells).

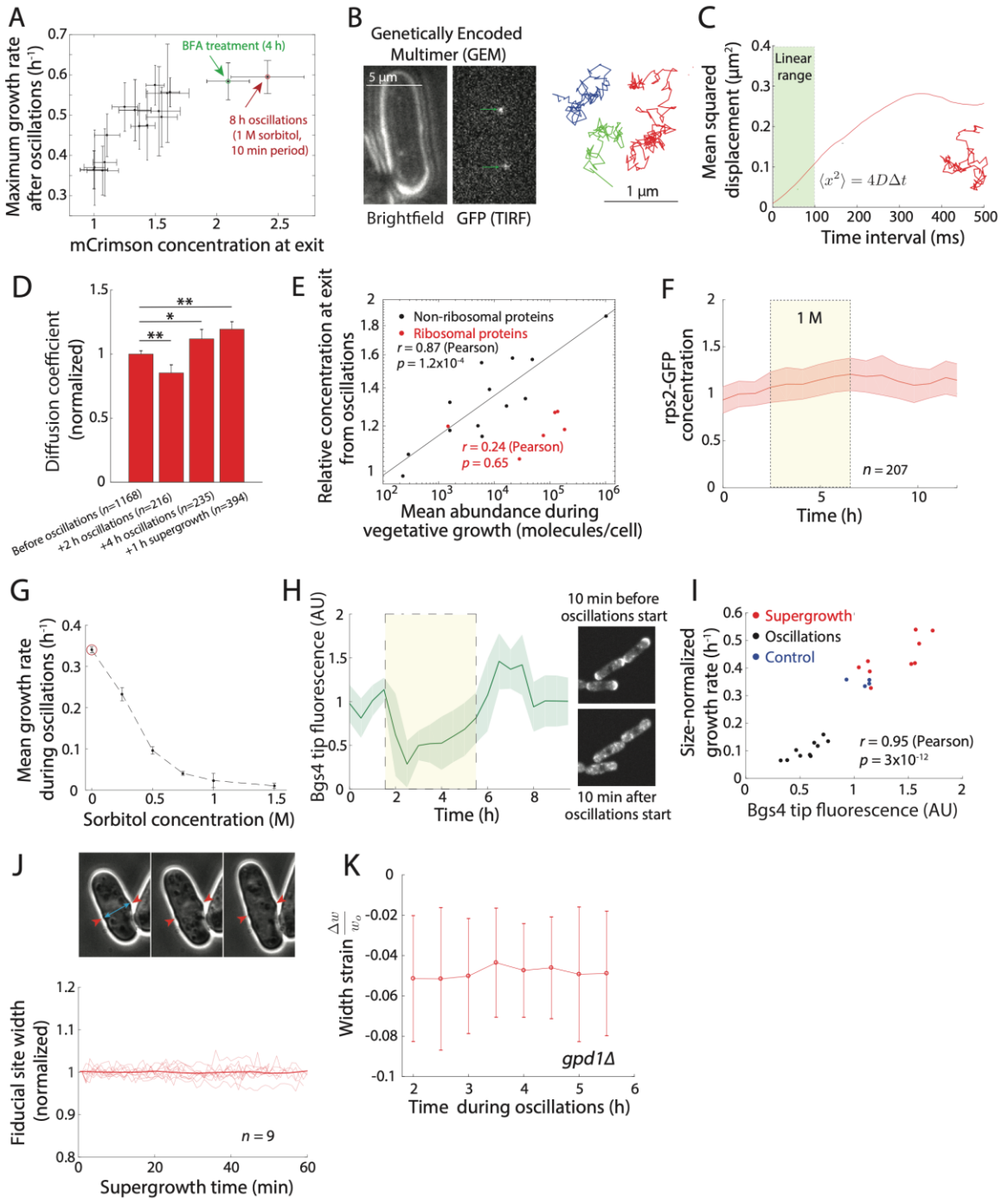

Figure S4: Cells during oscillations and supergrowth show increased levels of cell wall synthase at cell tips, but do not exhibit substantial differences in cytoplasmic crowding or cell-wall mechanics. (Related to Figures 5 and 6)

A) Maximal rates of supergrowth after osmotic shock oscillations correlate with increase in mCrimson protein concentration at exit from oscillations. Data include those from Figure 4, along with one point representing long-term (8 h), large-amplitude (1 M) osmotic shocks (red circle) and one point representing BFA-treated cells (green circle, Figure 6E). The highest supergrowth rate achieved was ~0.6 h^{-1}. Error bars are ±1 S.D. (n = 2714 cells).

B-D) Effect of oscillations on macromolecular crowding as assessed by microrheology using GEMs. (B) Left: Example of a single field of view during high-speed acquisition of GEM diffusion. GEMs appeared as diffraction-limited bright spots (circled) using total internal fluorescence (TIRF) microscopy. Right: Individual spots were tracked using the ImageJ Mosaic plugin for hundreds of milliseconds, typically the residence time of the GEM in the imaging plane. Tracks were filtered based on spot quality and length (STAR Methods). (C) Mean square displacement versus time for a representative GEM track. A typical track displayed diffusive and sub-diffusive behavior, captured through the anomalous diffusion coefficient (α). The linear range ($\alpha \sim 1$) is typically restricted to the first 100 milliseconds, in agreement with observations made in (Delarue et al., 2018). (D) GEM diffusion coefficients measured throughout an osmotic shock oscillation experiment (500 mM D-sorbitol, 10-min period, 4 h). Diffusion measurements were normalized to the mean diffusion coefficient prior to oscillations and were inferred from the first 100 ms of each track (STAR Methods). Error bars represent ±1 standard error of the mean (S.E.M.), and significance was measured by the two-sample Kolmogorov-Smirnov test. *: p<0.05, **: p<0.005.

E) Concentration increase of individual proteins scaled with their normal expression level. The concentration increase in non-ribosomal proteins during shocks was correlated with the log of protein abundance during steady-state growth, by contrast to ribosomal proteins for which the concentration increase was small and approximately independent of steady-state protein abundance.

F) The concentration of the ribosomal protein fusion rps2-GFP increased only modestly (<20%) during 1-M sorbitol oscillations that arrest growth almost completely. The 40S ribosomal protein S2 is encoded by a single essential gene (*rps2)*. The rps2-GFP fusion is a functional fusion, as it is able to support normal growth rate as the only rps2 protein in the cell. The dark centerline is the population-averaged cellular fluorescence (images acquired every 35 min), and the shading represents ±1 S.D. (n = 207 cells).

G) Mean elongation rate during shocks was inversely related to the amplitude of osmotic shock with D-sorbitol during oscillatory cycles with 10-min period and 4-h duration. Error bars are ±1 S.D. (n = 265 cells).

H-I) Osmotic oscillations increase the levels and polarization of the cell-wall glucan synthase Bgs4. (H) Left: Localization of 2GFP-Bgs4 at the cell tips during an oscillatory osmotic shock experiment. Yellow outlined box represents the 4-h duration of 0.5 M sorbitol shocks with 10-min period. Upon onset of oscillations, tip localization initially decreased by >70% (right), and re-localized concordant with the increase in growth rate during supergrowth. Shaded bars represent ± 1 S.D. (n = 64 cells). (I) Population-averaged size-normalized growth rate was highly correlated

with the level of 2GFP-Bgs4 tip localization during all phases of the experiment (r = 0.95).

J) Lack of cell width changes suggest that turgor did not change substantially during oscillations or supergrowth. (J) Top: Measurements of cell width at birth scars were used to assess changes in turgor. Red arrowheads mark a birth scar (raised edge of cell wall), which remains as a stable fiducial mark. Bottom: Cell width measured from birth scars at 10-s frame intervals remained approximately constant during supergrowth. The dark red line indicates the average of all trajectories. These data suggest that turgor did not change substantially (n = 9).

(K) Normalized width changes during hyperosmotic shocks of the osmotic response mutant (*gpd1Δ*) remained approximately constant throughout a typical oscillation experiment (500 mM D-sorbitol, 10-min period, 4 h), indicating that cell-wall properties remained approximately the same throughout the experiment. The mean response of ~5% agrees with previously published values (Atilgan et al., 2015). Error bars are ±1 S.D. (n = 84 cells).

Supplemental Movie Legends

Movie S1: Wild-type *S. pombe* cells exhibit supergrowth after osmotic shock oscillations. (Related to Figure 2) After 4 h of osmotic shock oscillations (0.5 M D-sorbitol, 10-min period, 24 cycles), cells exhibited supergrowth. Images were acquired with a frame interval of 1 min using phase-contrast imaging.

Movie S2: The concentration of mCrimson increases during oscillations and dilutes during supergrowth. (Related to Figure 5) FC3186 cells expressing mCrimson subjected to 4 h of osmotic shock oscillations (0.5 M D-sorbitol, 10-min period, 24 cycles), with subsequent supergrowth. Fluorescence images were acquired every 10 min (Methods).

Movie S3: Treatment with the secretion-inhibiting drug brefeldin A results in increased mCrimson concentration and subsequent supergrowth. (Related to Figure 6) FC3186 cells expressing mCrimson were subjected to treatment with 0.1 mg/mL brefeldin A for 4 h, during which time cell growth halted and mCrimson concentration increased. The drug was then washed out, and cells exhibited supergrowth and dilution of mCrimson.